forests

MDPI

Article

Improved Prediction of Forest Fire Risk in Central and Northern China by a Time-Decaying Precipitation Model

Jiajun Chen [1], Xiaoqing Wang [1,*], Ying Yu [2], Xinzhe Yuan [3], Xiangyin Quan [4] and Haifeng Huang [1]

[1] School of Electronics and Communication Engineering, Sun Yat-sen University, Guangzhou 510275, China; chenjj226@mail2.sysu.edu.cn (J.C.); huanhaifeng@mail.sysu.edu.cn (H.H.)
[2] Science Technology on Space Physics Laboratory, Beijing 100076, China; yyxk720@sina.com
[3] National Satellite Ocean Application Service, Beijing 100081, China; harley_yuan@mail.nsoas.org.cn
[4] China Academy of Launch Vehicle Technology, Beijing 100076, China; heavenmoonqxy@163.com
* Correspondence: wangxq58@mail.sysu.edu.cn

Abstract: With the increase in extreme climate events, forest fires burn in much larger areas. Therefore, it is important to accurately predict forest fire frequencies. Precipitation is an important factor that affects the probability of future forest fires. Previous models used average precipitation values, but the attenuation of precipitation was not considered. In this study, a time-decaying precipitation algorithm was used to calculate the comprehensive precipitation index. This method can better represent the effect of precipitation in predicting the occurrence of forest fires. Moreover, observed fire spots were converted into a continuous density of fire spots. The structure of the prediction model is more realistic, which is conducive to obtaining higher-precision prediction results. Additionally, the support vector machine (SVM) regression model was used to construct a forest fire warning model. When the comprehensive precipitation index was compared with the average precipitation value, the accuracy of the four forest areas in central and northern China in the test set was improved by approximately 10%. The findings are relevant to forest ecologists and managers for future mitigation of forest fires, and also for successful prediction of other fire-prone areas.

Keywords: time-decaying model; forest fire warning model; SVM regression model; moderate-resolution imaging spectroradiometer (MODIS)

check for updates

Citation: Chen, J.; Wang, X.; Yu, Y.; Yuan, X.; Quan, X.; Huang, H. Improved Prediction of Forest Fire Risk in Central and Northern China by a Time-Decaying Precipitation Model. *Forests* **2022**, *13*, 480. https://doi.org/10.3390/f13030480

Received: 22 January 2022
Accepted: 17 March 2022
Published: 19 March 2022

1. Introduction

Forest fires are unavoidable and play an important role in environmental transformation in a wide variety of ecosystems [1,2]. In recent years, with global warming and frequent extreme weather events, forest fire damage is worse in China than it was five years ago, which has increased the negative effects on the environment, human values, and society in many countries [3]. In addition, many countries are also facing the same situation. In 2019, there were 50,477 forest fires in the United States, covering a total area of more than 1.8 million hectares. Australia experienced a long and severe fire season in the second half of 2019, with approximately 7 million hectares of land being burned [4]. Northeast China is also one of the hardest hit areas by forest fires, with severe forest fire losses. In 2018 and 2019, severe and catastrophic forest fires occurred respectively, causing severe harm to forest resources, terrestrial ecosystems, and even the achievements of ecological civilization construction [5]. In the future, due to the increase in extreme climate and global warming, forest fires will become more frequent. Therefore, building a high-accuracy forest fire warning model is particularly important.

Exploring wildfire drivers is essential for constructing forest fire warning models. Some forest fire warning models use meteorological data to predict forest fires frequencies, such as the Canadian Forest Fire Danger Rating System (CFFDRS) [6] and the National Forest Fire Risk System (NFDRS) [7]. Forest fire warning models such as multivariate adaptive regression splines are optimised using the differential flower pollination (MARS-DFP) model [8]. The framework of Chuviecoa et al. for fire risk assessment [1] incorporates remotely sensed data into the impact factors of forest fire warning models. Müller et al. used weather data, a fuel map, topography, and other data to construct an integrated fire danger assessment system (IFDS) [9]. Zhong et al. used weather data, land cover data, and human activity data to predict forest fire risk [10].

In the process of selecting the characteristic factors that affect the forest fire warning model, most of the previous models selected precipitation as an important characteristic factor of the model. A negative correlation exists between the precipitation value and the occurrence of forest fires [11]. The status of vegetation water is another important factor in the detection of forest fire behaviour. Moreover, precipitation is an important factor affecting the state of vegetation water [12]. Zhang et al. [13] used a convolutional neural network (CNN) model to establish a forest fire sensitivity model. That study illustrated that the importance of precipitation in the model was ranked fourth. Mohajane et al. [14] used a random forest model to predict the occurrence of forest fires, and precipitation was ranked as the second most important factor out of more than a dozen factors. These results show that the precipitation value plays an important role in the prediction of the forest fire danger rating level.

The acquisition of precipitation data currently relies mainly on three forms: direct observations, radar measurements, and satellite inversion data [15]. Direct observations are mainly obtained from rain gauges distributed near meteorological stations worldwide and are the most direct and accurate. However, owing to the influence of natural and economic conditions, the spatial distribution of meteorological stations is extremely uneven, making it difficult to comprehensively observe the spatial distribution of precipitation. Radar measurements rely mainly on the application of weather radar. Its principle is to determine the position and characteristics of the target based on the reflection of the target to the radar wave. Compared with direct observations, radar measurements have a wider detection range and stronger detection performance, but they are easily affected by factors such as technical conditions, electronic signals, and the operating environment. Large errors still exist in complex terrain environments. Satellite inversion relies mainly on the use of meteorological observation satellites. This is an emerging technical approach and has the advantage of wide coverage, high continuity, high temporal and spatial resolution, and a short observation period, especially for some non-observed data. Tropical Rainfall Measuring Mission (TRMM) satellites are used to monitor and study precipitation in tropical and subtropical regions. The new generation of Global Precipitation Measurement (GPM) satellites have inherited the advantages of the older generation of TRMM satellites. This improves the data correction algorithm and microwave detection technology. At the same time, the accuracy of GPM precipitation products in areas with complex terrain and high-altitude mountainous areas was higher than that of multi-satellite precipitation analysis (TPMA) and Coastal Ocean Research and Monitoring Program (CORMP) precipitation products. The Integrated Multisatellite Retrievals for GPM (IMERG) are a grade 3 precipitation product of GPM. IMERG currently provides three series of precipitation data: early, late, and final runs. In terms of the spatial distribution of precipitation, the performance of IMERG-final precipitation products is better than that of TRMM. This is because GPM precipitation products have higher accuracy owing to the fine-scale time and space resolutions [16]. The precipitation data used in this study are the "final-run" products of GPM_3IMERGDF. The dataset is derived from GPM_3IMERGHH every 30 min. The result obtained represents the final estimated value of daily accumulated precipitation, with an accuracy of 1 d and $0.1^{\circ} \times 0.1^{\circ}$.

In previous forest fire prediction models, Bui et al. [8] and Nguyen et al. [17] used the MARS-DFP model and advanced machine learning algorithm models, respectively, in which annual average precipitation, monthly average precipitation, and drought days were selected as the precipitation values. The disadvantage of this method is that the time interval between the precipitation date and the forecast date and the attenuation of precipitation were not considered. Because of water loss effects, such as evaporation and infiltration, an earlier precipitation time has less impact on future forest fire risk. Therefore, in this study, the precipitation data used the time-decay model to calculate the comprehensive precipitation index. The time-decaying precipitation algorithm can better reflect the impact of precipitation on the forest fire warning model.

Regarding the selection of the forest fire warning model, previous studies used a linear addition model in their forest fire warning models [18–20]. However, the impact of forest danger factors on forest fires is not a simple linear combination. Forest fires are naturally complex and follow a non-linear process [21]. As the advantages of machine learning have attracted increasing attention, machine learning is increasingly being used to predict forest fire frequencies, such as frequency ratio random forest [14], random forests [22–24], and the multilayer perceptron neural network (MLP-Net) [17]. Forest fires are regional events that affect the surrounding environment. However, these forest fire warning models are mostly classified as models that treat forest fire data as discrete points and the location of the ignition point is often uncertain. The use of fire density can overcome this limitation [25]. Some models convert discrete fire spots into a continuous density of fire spots. Monjarás-Vega et al. used geographically weighted regression (GWR) to predict fire density [26] by dividing the number of fire records within a pixel by the pixel area (km^2). Oliveira et al. used two regression methods, multiple linear regression, and random forest regression models to simulate fires in the European Mediterranean region. The random forest regression results were higher than 92% [23].

This study aims to build a high-accuracy forest fire warning model based on a comprehensive precipitation model, using a support vector machine (SVM) regression model with a Gaussian kernel. Comparisons will be made with other machine learning models to measure the generalisation ability and robustness of the model. In addition, this study will attempt to convert discrete fire spots into a continuous density of fire spots through Gaussian convolution. The findings will be used to improve the accuracy of forest fire prediction, which is critically important for the successful mitigation of increasingly common forest fires owing to climate change.

2. Materials and Methods

In this section, we first introduce how the forest fire density was obtained using a Gaussian convolution kernel. Second, we show how the precipitation data was obtained and how the time-decaying precipitation algorithm was used to calculate the comprehensive precipitation index. A random forest model was then used to filter the selected factors. Finally, we introduce the regression model used in this study and the generated forest fire danger rating map, which is the SVM regression model based on a Gaussian kernel. A flow chart of this study can be seen in Figure S1 in the Supplementary Materials.

2.1. Fire Spots Density Map Generation

The historical fire data used in this study were obtained from the global forest fire historical data website provided by NASA (https://firms.modaps.eosdis.nasa.gov/map/), when we obtained it on 5 October 2021. The records mainly come from the MCD14DL products of the Terra and Aqua satellites. We first identified forest fires that occurred in central and northern China in recent years. Thereafter, we determined the corresponding geographic location and the time at which forest fires occurred. Finally, the data were filtered with a fire spots confidence higher than 60%.

The data form of the forest fire spots is a scatter diagram of the forest area. However, the location of the forest fire spots was uncertain. The use of forest fire density can overcome this limitation. In this study, the scatter plot of forest fire spots was transformed into a forest fire density map. The data points of each forest area were considered as the values of the surrounding data. The closer to the forest fire, the greater the surrounding area that will be affected by the forest fire. The definition of convolution is to set $f(x)$ and $g(x)$ as integrable functions on the domain, which can then be calculated using Equation (1).

$$f(x) * g(x) = \int_{-\infty}^{\infty} \int_{-\infty}^{\infty} f(u,v) g(x-u, y-v) du dv \tag{1}$$

In this study, a two-dimensional Gaussian convolution kernel was used for convolution, and the expression of the two-dimensional Gaussian function was $g(x,y) = \frac{1}{2\pi\sigma^2} e^{-(x^2+y^2)/2\sigma^2}$, where σ is the convolution range. This expression satisfies the convolution requirements described above. Oliveira et al.'s model uses a 10 km range for convolution of the fire density. Thus, this study also used a 10 km range as the convolution. In addition, the value of σ was taken as 10 after selection. This enabled the scattered forest fire spots map to be converted into a forest fire density map, which facilitated the establishment of the subsequent regression model. Figure S2a,b in the Supplementary Materials show the fire spots in the forest area in the southern part of the Greater Khingan Mountains from 29 March to 13 April 2018, and the density of fire spots in the forest area after convolution. We use yellow as the color with the largest density value, and blue as the color with the smallest density value. The closer the color to yellow, the larger the density value it represents.

2.2. Obtaining Precipitation Data

The Global Rainfall Observation Satellite currently consists of ten satellite clusters. Its core observation platform was launched on 28 February 2014. The precipitation estimates obtained by the various precipitation-related passive microwave (PMW) sensors that make up the GPM constellation were calculated using the Goddard profiling algorithm (GPROF). IMERG, a grade 3 precipitation product of GPM, provided three series of precipitation data: ″early-run″, ″late-run″, and ″final-run″. The IMERG ″early-run″ data are released with a lag of approximately 4 h in the observation time. It provides relatively fast results for flood analysis and other short-term applications. The IMERG ″late-run″ publishes a lag in the observation time of approximately 14 h, which is suitable for daily and long-term applications, such as crop forecasting. Once the monthly scale rain gauge data of the GPCC are collected, the estimated precipitation is corrected to generate the IMERG ″final-run″ data. The lag time for the release of this series of data was approximately 3–4 months. These three series all produce products (3IMERGHH) with a time-space resolution of 30 min and $0.1° \times 0.1°$. Comparing the real-time "early-run" and "late-run" IMERG products of GPM satellites, the "final-run" products had the highest accuracy for regional precipitation estimation. At the same time, GPM satellites significantly enhanced the capture rate of weak precipitation times. Compared with TRMM precipitation products, GPM precipitation data had a higher correlation with the measured precipitation on a daily scale. At the same time, in some areas, the correlation coefficient between GPM satellite precipitation data and observations was high, the error range was small, and the root mean square error was low. When compared with the TMPA precipitation products, the IMERG-final of the GPM proved to be more appropriate for capturing heavy precipitation. Furthermore, for the southwestern part of India affected by the monsoon season, IMERG products are more able to reflect the monsoon cloudburst characteristics of the study area than GSMaP precipitation products. In terms of the spatial distribution of precipitation, the performance of IMERG-final precipitation products was better than that of TRMM precipitation products. This is because the GPM precipitation products have a higher accuracy and the time and space resolution of the GPM precipitation products is finer, which has certain advantages [15].

The precipitation data used in this study was the "final-run" product of GPM_3IMERGDF. The dataset was derived from GPM_3IMERGHH every 30 min. The results obtained represent the final estimate of daily accumulated precipitation. The dataset was generated at NASA Goddard Geosciences (GES) Data and Information Service Centre (DISC) by summing the effective precipitation retrieval in GPM_3IMERGHH that day and presenting it in millimetres (mm). The accuracy was 1 d, and $0.1^{\circ} \times 0.1^{\circ}$.

2.3. Time-Decaying Precipitation Algorithm

Previous forest fire prediction models used drought days or monthly average precipitation as the value of precipitation. The above two methods can represent the impact of precipitation data on forest fires to a certain extent. However, these methods average the weight of daily precipitation and do not consider the impacts of precipitation on different dates. In this study, we assumed that the precipitation value of the preceding few days affected the occurrence of future forest fires. The longer the time, the smaller the contribution of precipitation. Therefore, in this study, the comprehensive precipitation index was calculated using a time-decaying precipitation algorithm.

In a time-decaying model [27], the descending magnitude of the numerical value is proportional to its time. It can be expressed as the following differential equation, Equation (2), where N is the numerical value, t represents time, and γ is the decay constant.

$$\frac{dN}{dt} = -\gamma N \tag{2}$$

Applying Equation (2) to the precipitation value results in

$$N(t) = N_0 e^{-\gamma t} \tag{3}$$

where, $N(t)$ is a quantity related to time t, which represents the contribution of precipitation t-days earlier. N_0 represents the precipitation value on day t.

With the comprehensive addition of precipitation on n days, $D_{Precipitation}$ is the value of the comprehensive precipitation, where the coefficient adopts $e^{-A(t-1)}$ defined by the time-decay function, t is the number of days, D_t is the precipitation on t days earlier, and A is the undetermined constant term.

$$D_{Precipitation} = \sum_{t=1}^{n} e^{-A(t-1)} * D_t \tag{4}$$

It is necessary to determine the value of the undetermined constant A and the precipitation value of the previous n days. Mutual information can represent the amount of information contained in one random variable by another random variable, which can be used to measure the correlation between them and is not limited to linear relationships. The formula for mutual information is as follows:

$$I(X;Y) = \sum_{x \in X} \sum_{y \in Y} p(x,y) log \frac{p(x,y)}{p(x)p(y)} \tag{5}$$

where, $p(x,y)$ is the joint probability distribution function of X and Y, and $p(x)$ and $p(y)$ are the marginal probability distribution functions of X and Y, respectively.

In this study, the authors used data from the forest area near the Oroqen Autonomous Banner area on 4 April 2016, from the northern Greater Khingan Mountains on 1 April 2017, and around Mohe City on 20 April 2016, to determine the A value and select the precipitation data of the previous n days. Figure 1 shows the mutual information value between different comprehensive precipitation indices and forest fire density, where the comprehensive precipitation index is the different combinations of the constant A value and the previous n days' precipitation value. As shown in Figure 1, when A is 0.1657 and the precipitation value of the previous three days is selected, the mutual information value of comprehensive precipitation and forest fire density is the largest. Therefore, in this study, $A = 0.1657$ and $n = 3$.

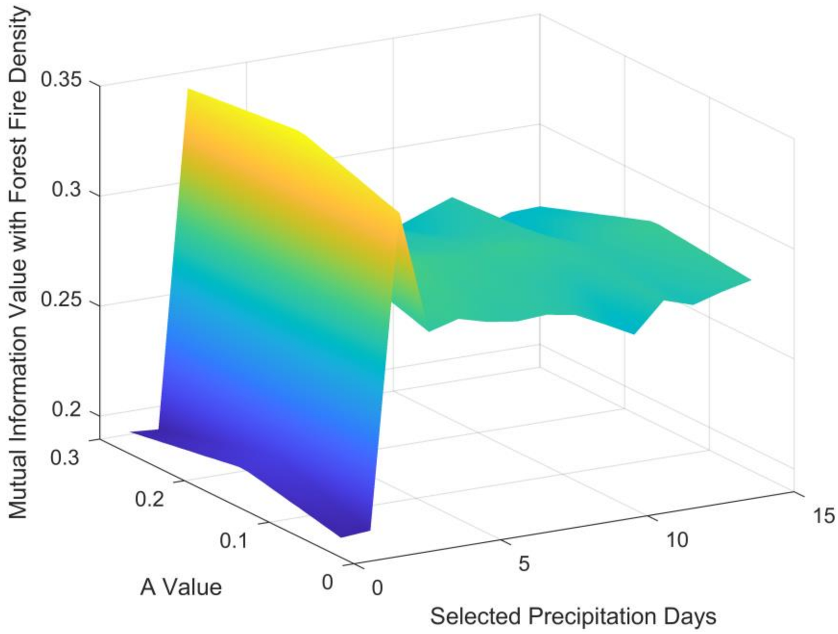

Figure 1. Mutual information value between different comprehensive precipitation index and forest fire density.

If the monthly average precipitation data are used as the precipitation value, the mutual information value between the monthly average precipitation data and the forest fire density is approximately 0.1729. It can be observed that the comprehensive precipitation index obtained by the time-decaying precipitation algorithm has a better correlation with the forest fire density, which can predict forest fires more accurately.

2.4. Independent Variables and Feature Selection

The climatic characteristics of an area influence the occurrence and intensity of forest fires [28]. Regarding climatic factors, variations of air temperature and wind speed have found influencing severity and frequency of forest fires, whereas variation of rainfall influences soil moisture and drought [28–31]. Altitude was considered because it influences solar radiation, temperature, and evapotranspiration of the terrain, which are indirectly related to forest fires [32]. Most forest fire warning models choose to use weather data, geographic data, and vegetation data as characteristic factors [5,17,21]. Therefore, in this study, the impact factors included the maximum daily temperature, daily maximum wind speed, visibility, comprehensive precipitation index, relative humidity, altitude, slope, the normalized difference vegetation index (NDVI), and the vegetation supplication water index (VSWI). The daily maximum temperature, daily maximum wind speed, visibility, precipitation, and relative humidity data were obtained from local weather stations. Topography plays an important role as it can control the distribution of vegetation and wind speed. It also has an important role in the precipitation and soil moisture [33,34]. The altitude and slope data were obtained using SPTMDEM 90M elevation data.

The vegetation coverage rate of the forest was represented by the NDVI. NDVI reflects the growth status that is a proxy for fuel load distribution [21,35]. The NDVI was calculated using the reflection value of the near-infrared and infrared bands, and by using the reflectance data of bands 1 and 2 in the MOD021KM remote sensing data. The formula for calculating the NDVI is:

$$NDVI = \frac{\rho_{NIR} - \rho_R}{\rho_{NIR} + \rho_R} \quad (6)$$

The value range of NDVI is $[-1, 1]$. A negative value implies that the ground is covered by clouds, water, snow, etc., while a positive value implies vegetation coverage. This value increased with an increase in coverage.

The VSWI can, to a certain extent, reflect the growth status of crops and the moisture content of vegetation [36], and can be expressed as:

$$VSWI = \frac{NDVI}{Ts} \quad (7)$$

where Ts is the surface temperature. The Ts data were obtained from MOD11A2 remotely sensed data, which recorded eight days of comprehensive land surface temperature. The larger the VSWI value, the higher the vegetation moisture content.

Figure S3a–f in the Supplementary Materials show the daily maximum wind speed, daily maximum temperature, NDVI, relative humidity, altitude, and VSWI in the forest area near the Oroqen Autonomous Banner, from 4 April 2016, and of some forest areas in the training dataset used in this study, respectively.

In this study, the selected feature factors were filtered to determine whether they have an impact on the occurrence of forest fires. Because the regression SVM model is non-linear, the random forest feature importance measurement method was used for filtering [37].

A random forest can measure the importance of each feature, and feature extraction is mainly based on the out-of-bag (OOB) principle. This principle implies that if a certain feature is important, the accuracy of the model of adding noise to this feature on the model is quite different from that without adding noise to this feature. The importance of meteorological and geographic factors to fire density is shown in Figure 2.

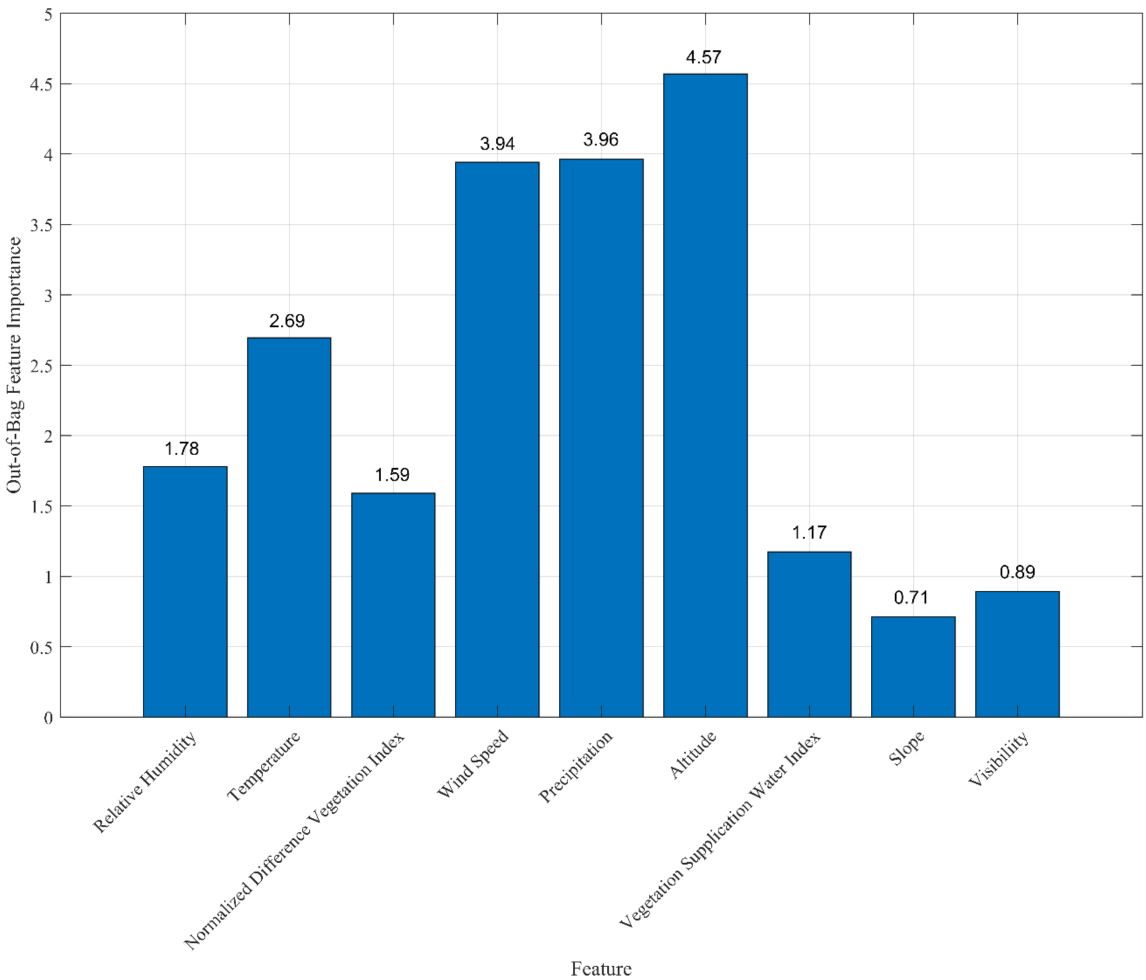

Figure 2. Importance of factors to the fire density.

As shown in Figure 2, except for slope and visibility, the importance of the OOB feature values of the other feature factors was greater than 1. Therefore, in the selection of characteristic factors, only the relative humidity, daily maximum temperature, NDVI, daily maximum wind speed, precipitation, VSWI value, and altitude were chosen.

2.5. SVM Regression Model

The objective function of the SVM regression model is:

$$\begin{gathered} min\frac{1}{2}\parallel \omega \parallel^2 + C\sum_{i=1}^{m}(\xi_{1i}+\xi_{2i}) \\ s.t. -\varepsilon-\xi_{1i} \le y_i - \left(\omega^T\varphi(x_i)+b\right) \le \ \varepsilon+\xi_{2i} \\ \xi_{1i} \ge 0,\ \xi_{2i} \ge \ 0\ (i=1,2,\ldots m) \end{gathered} \tag{8}$$

where ω is the weight vector of the output space, $\varphi(x_i)$ is the non-linear mapping from the input space to the output space, ξ_{1i}, ξ_{2i} are slack variables, b is the offset value, and ε is the insensitive range of the loss value.

The loss function measurement of the SVM regression model is:

$$err(x_i,y_i) = \begin{cases} 0 & \left|y_i-\left(\omega^T\varphi(x_i)+b\right)\right| \le \ \varepsilon \\ \left|y_i-\left(\omega^T\varphi(x_i)+b\right)\right|-\varepsilon & \left|y_i-\left(\omega^T\varphi(x_i)+b\right)\right| > \ \varepsilon \end{cases} \tag{9}$$

According to the above formula, the objective function of SVM regression is:

$$min_{\omega,b,\xi_{1i},\ \xi_{2i}} max_{\mu_1,\mu_2,\alpha_{1i}\ge 0,\alpha_{2i}\ge 0} L(\omega,b,\mu_1,\mu_2,\alpha_{1i},\alpha_{2i},\xi_{1i},\xi_{2i}) \tag{10}$$

where $\mu_1,\mu_2,\alpha_{1i},\alpha_{2i}$ are Lagrangian multipliers.

This optimisation goal satisfies the Karush–Kuhn–Tucker (KKT) condition, implying that the optimisation problem was solved by transforming the Lagrangian duality into an equivalent dual problem.

$$max_{\mu_1,\mu_2,\alpha_{1i}\ge 0,\alpha_{2i}\ge 0} min_{\omega,b,\xi_{1i},\ \xi_{2i}} L(\omega,b,\mu_1,\mu_2,\alpha_{1i},\alpha_{2i},\xi_{1i},\xi_{2i}) \tag{11}$$

This was achieved by first calculating the minimum value of the function for $\omega, b, \xi_{1i},\ \xi_{2i}$ and then calculating the maximum value of the Lagrange multipliers $\mu_1,\mu_2,\alpha_{1i},\alpha_{2i}$ to determine the corresponding SVM regression model function [38].

3. Results and Discussion

3.1. SVM Model Training and Testing

In this study, four forest areas in central and northern China were selected as the training and test sets of the model.

After the feature selection was completed, the filtered dataset was put into the SVM regression model for training. The independent variables in the dataset were the relative humidity of the forest area, daily maximum temperature, daily maximum wind speed, the comprehensive precipitation index, NDVI, VSWI, and altitude of the forest area. The dependent variable was fire density in the forest area. The NDVI, VSWI, and altitude data are continuous in the forest area, and each point in the forest area has a value. The relative humidity, daily maximum temperature, daily maximum wind speed, and precipitation data were selected from the local weather station, so the data were discrete in the forest area. In this study, the Kriging algorithm was used to linearly interpolate the above-mentioned meteorological data. In addition, the discrete fire spots were converted into continuous forest fire density data through the Gaussian convolution kernel. All feature factor data were normalised so that the resolution of the data was unified. The precipitation value was selected from the data of the first three days of forest fire forecasting. Other meteorological data, NDVI, and altitude were selected from the daily forest area data. This selection was based on the timeliness of the data. Forest fires were selected for the next 15 days.

The ratio of forest fire spots density data and non-fire data in the training set was approximately 1:1, which prevented the difference in two of them from causing the model to overfit. Non-fire data were randomly selected in the forest area. The SVM kernel function selects the Gaussian kernel, and the data are normalised. In addition, the kernel scale was specified as three after selection.

The trained SVM regression model was used in the test set to obtain the forest fire density data in the prediction set area. These test sets are the forest area in the southern part of Greater Khingan Mountains on 29 March 2018, the forest area near Hulunber City on 21 March 2015, the forest area near Chongqing city on 8 March 2013, and the forest area near TongLiao city on 25 February 2019. Figures S4a,b–S7a,b in the Supplementary Materials show the predicted fire density map and actual fire density map of the four concentrated forest areas over the following 15 days. In Figures S4a,b–S7a,b in the Supplementary Materials, we use yellow as the color with the largest value, and blue as the color with the smallest value. The closer the color to yellow, the larger the value it represents. As can be seen from Figures S4a,b–S7a,b in the Supplementary Materials, the areas with high density of actual forest fires are basically in the areas with high density of predicted forest fires frequencies.

After training the SVM model with the training set data, the resubLoss function was used to verify the SVM regression model. The interpretation of the resubLoss function depends on the mean squared error and weighting scheme. In general, better models yield smaller loss values. The error obtained in this model was small, approximately 0.68.

The data of the forest area near Hulunber city on 21 March 2015 in the test set were used as an example to analyse the impact of parameters on forest fires. Figure S8a–h shows the relative humidity, daily maximum temperature, daily maximum wind speed, the comprehensive precipitation index, NDVI, VSWI, and altitude of the forest area near Hulunber City and the predicted fire density over the following 15 days. As shown in Figure S8a–h, the predicted high value of forest density is concentrated in areas with higher daily maximum temperature, higher daily maximum wind speed, and lower relative humidity, indicating that under these conditions, the higher the probability of forest fires. In addition, Figure S8a–h show that the lower the comprehensive precipitation index, the higher the probability of forest fires. Regarding the effects of NDVI and VSWI on forest fires, forest fire densities with larger values were observed in areas with higher vegetation density and higher water content. Figure S8a–h also shows that areas with a higher density of forest fires are located at lower altitudes.

In this study, the natural breakpoint method [13] was used to classify the forest fire danger rating level, and the natural breakpoint method was used as a clustering method. Its main idea is to maximise the similarity within each group, while the dissimilarity between the external groups is the greatest. According to the density of forest fire spots in the area and the natural breakpoint method, the forest fire danger rating is divided into five levels according to the density of forest fire spots, as shown in Table 1.

Table 1. Classification of forest fire danger rating map.

Fire Risk Rating	One	Two	Three	Four	Five
Fire density	$(-\infty, 0)$	$[0, 0.19)$	$[0.19, 0.54)$	$[0.54, 0.94)$	$[0.94, \infty)$

After dividing the forest fire rating level, the forest fire danger rating maps of the forest areas and the predicted fire spots in these areas over the following 15 days are shown in Figure 3a–d, where the red points indicate the actual fire spots.

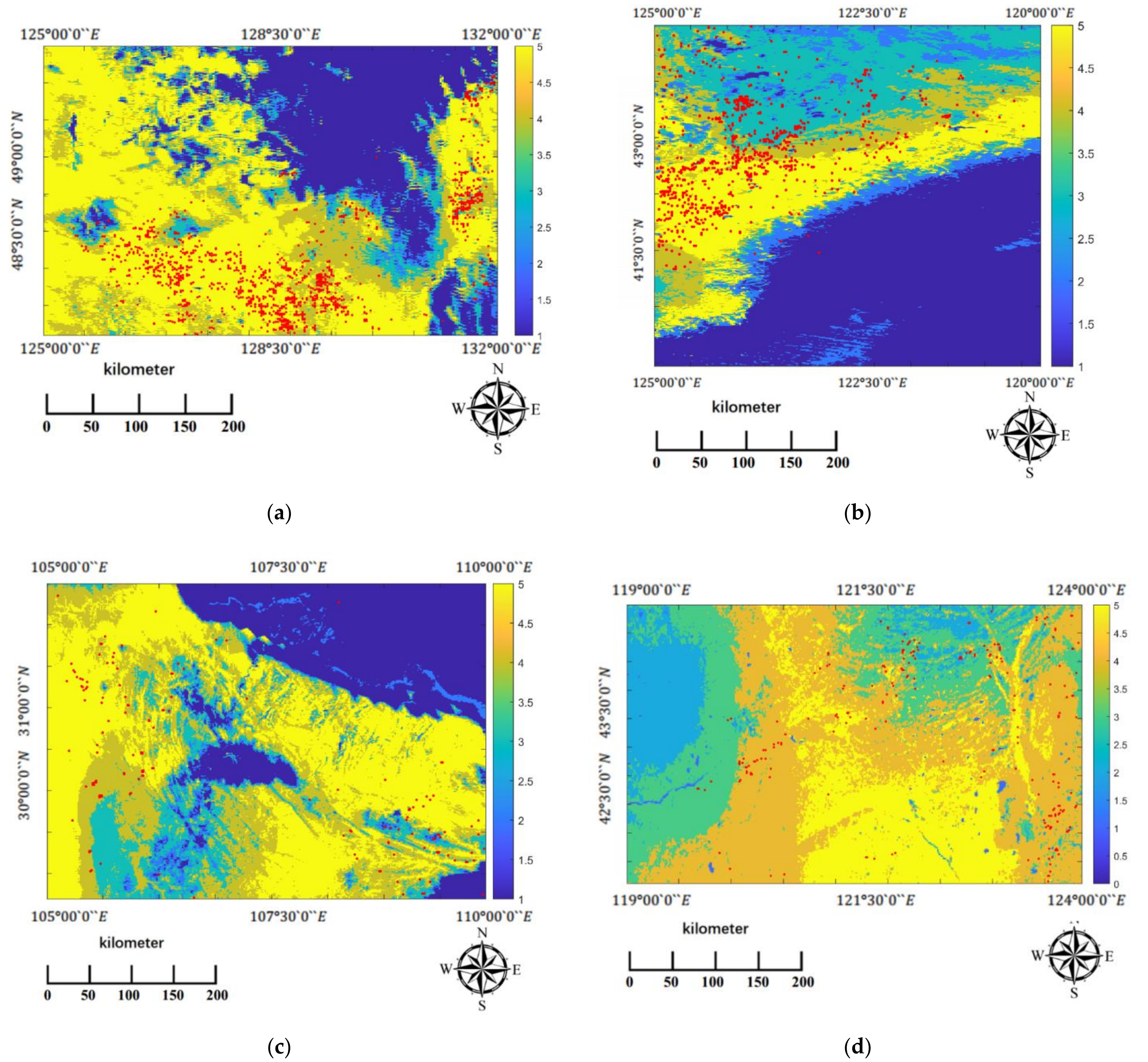

Figure 3. Forest fire danger rating map constructed by the Support Vector Machine (SVM) regression model established in this study. (**a**) Fire risk grade map of the forest area in the southern Greater Khingan Mountains; (**b**) forest area near Hulunber city; (**c**) forest area near Chongqing city; (**d**) forest area near Tongliao city.

The proportion of forest fire points in the test set falling on each fire danger rating map is shown in Figure 4.

Figures 3a–d and 4 show that most of the forest fires are concentrated on fire danger rating levels 3, 4, and 5, while only a small proportion of the fires are at fire danger rating levels 1 and 2. If an area with a rating of level 3 or higher is used to predict the occurrence of fire [39], the accuracy rate of the regression model established by the test set in this study, is approximately 0.98, 0.99, 0.95, and 0.93, respectively. The test sets are the forest area in the southern Greater Khingan Mountains, the forest area near Hulunber City, the forest area near Chongqing City, and the forest area near Tongliao city.

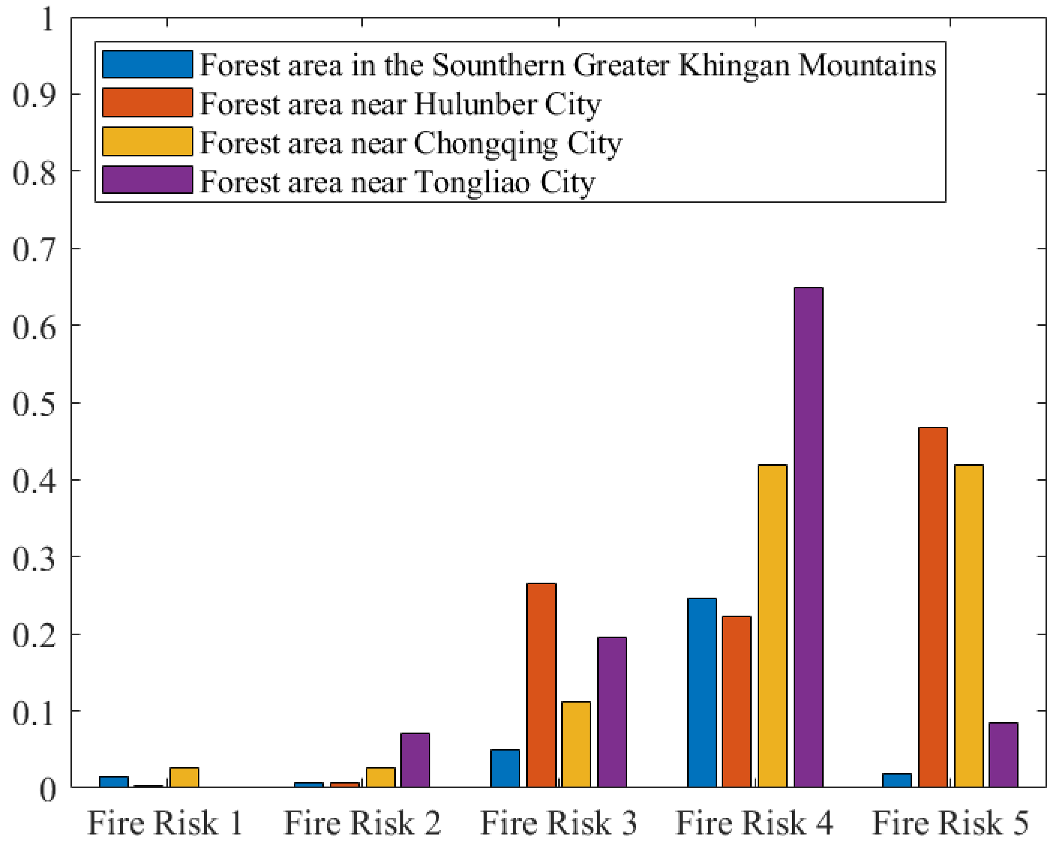

Figure 4. Proportion of forest fire spots falling on each fire danger rating map.

3.2. Comparison with Various Forest Fire Prediction Model

This study is optimized for considering the influence of precipitation on the fire frequency. Therefore, it is necessary to confirm that the selection of the comprehensive precipitation index can indeed improve the accuracy of forest fire warning by comparing the selection of precipitation data. The monthly average precipitation data are used as the precipitation factor in the regression model; the test set result obtained by the model trained with this dataset is shown in Figure 5a–d, where the red points are the actual fire spots.

As can be seen from Figure 5a–d, compared with the use of the comprehensive precipitation index to build the model, although most of the forest fires predicted by this model fall above the fire danger level three, the total number is less than that using the comprehensive precipitation index.

Subsequently, the test set results are compared with the results of this study. Figure 6a–d show the proportion of fire points in four different forest areas in the test set using two different methods that fall within the forest fire danger rating map.

Using these two different methods, results of the accuracy of the fire prediction of these areas in the test set are shown in Table 2. When compared with the monthly average precipitation, using the comprehensive precipitation index as the precipitation data, the accuracy of predicting forest fires increased by approximately 10%. This shows that the method proposed in this study to represent precipitation data can better reflect the impact of precipitation on forest fires.

Table 2. Accuracy of the test sets using two different methods.

	Test 1	**Test 2**	**Test 3**	**Test 4**
Comprehensive Precipitation Index	0.98	0.99	0.95	0.93
Monthly Average Precipitation	0.91	0.79	0.73	0.89

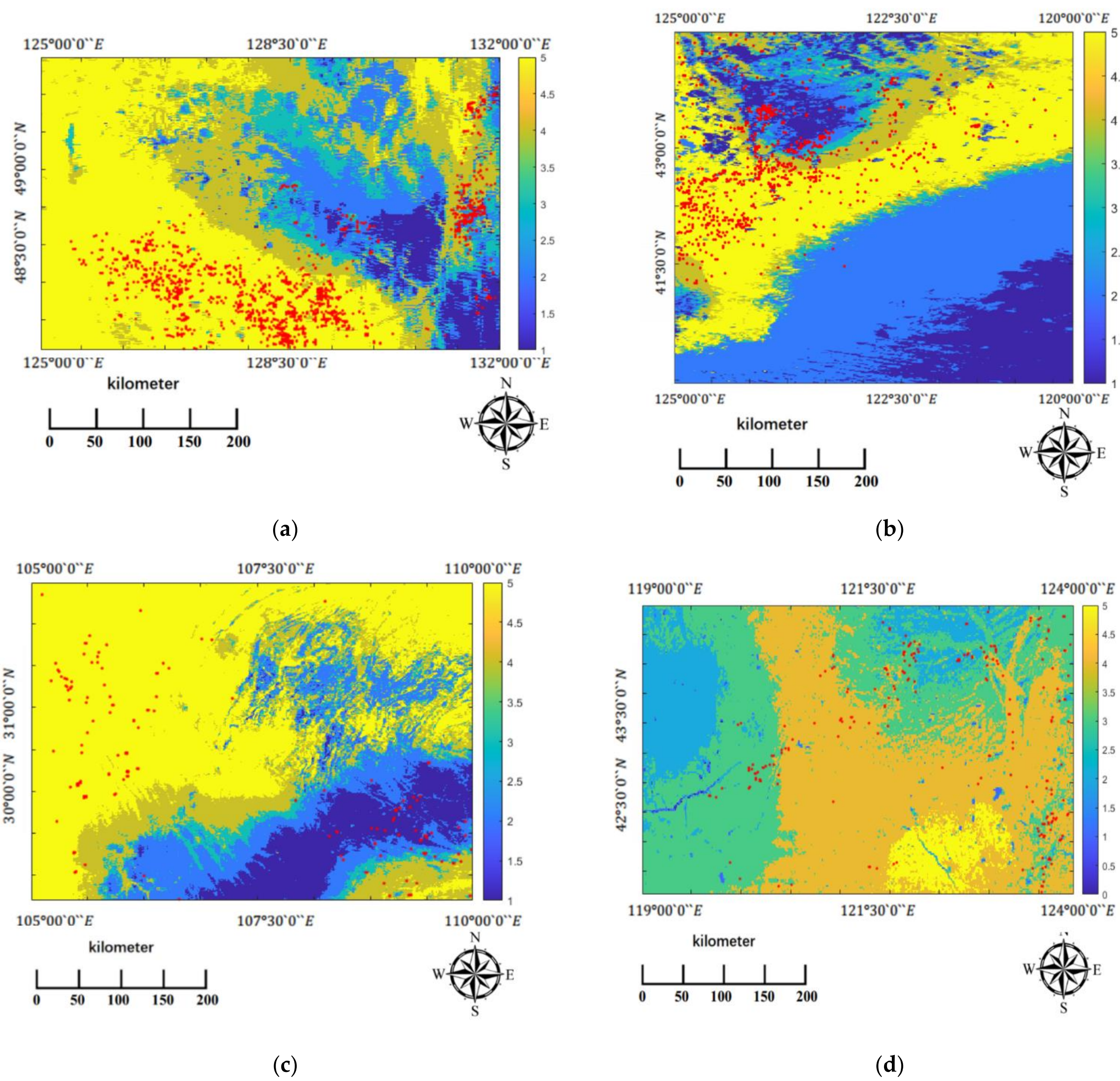

Figure 5. Forest fire danger rating map constructed by the SVM regression model using monthly precipitation data: (**a**) forest area in the southern Greater Khingan Mountains; (**b**) forest area near Hulunber city; (**c**) forest area near Chongqing city; (**d**) forest area near Tongliao city.

In the forest fire warning model and forest-related prediction model, logistic regression produces good effects and is commonly used in statistical methods [24,40]. Among the machine learning models, the artificial neural network (ANN) is effective in the forest fire early warning model [41–43]. In this study, a logistic regression model [44] and ANN [42,43,45] were used to predict the forest fire danger rating map in the same forest area. These two models were compared using the regression model established in this study.

The forest fire danger rating chart defined by the probability predicted by the logistic regression model is shown in Figure 7a–d, where the red points indicate the fire spots.

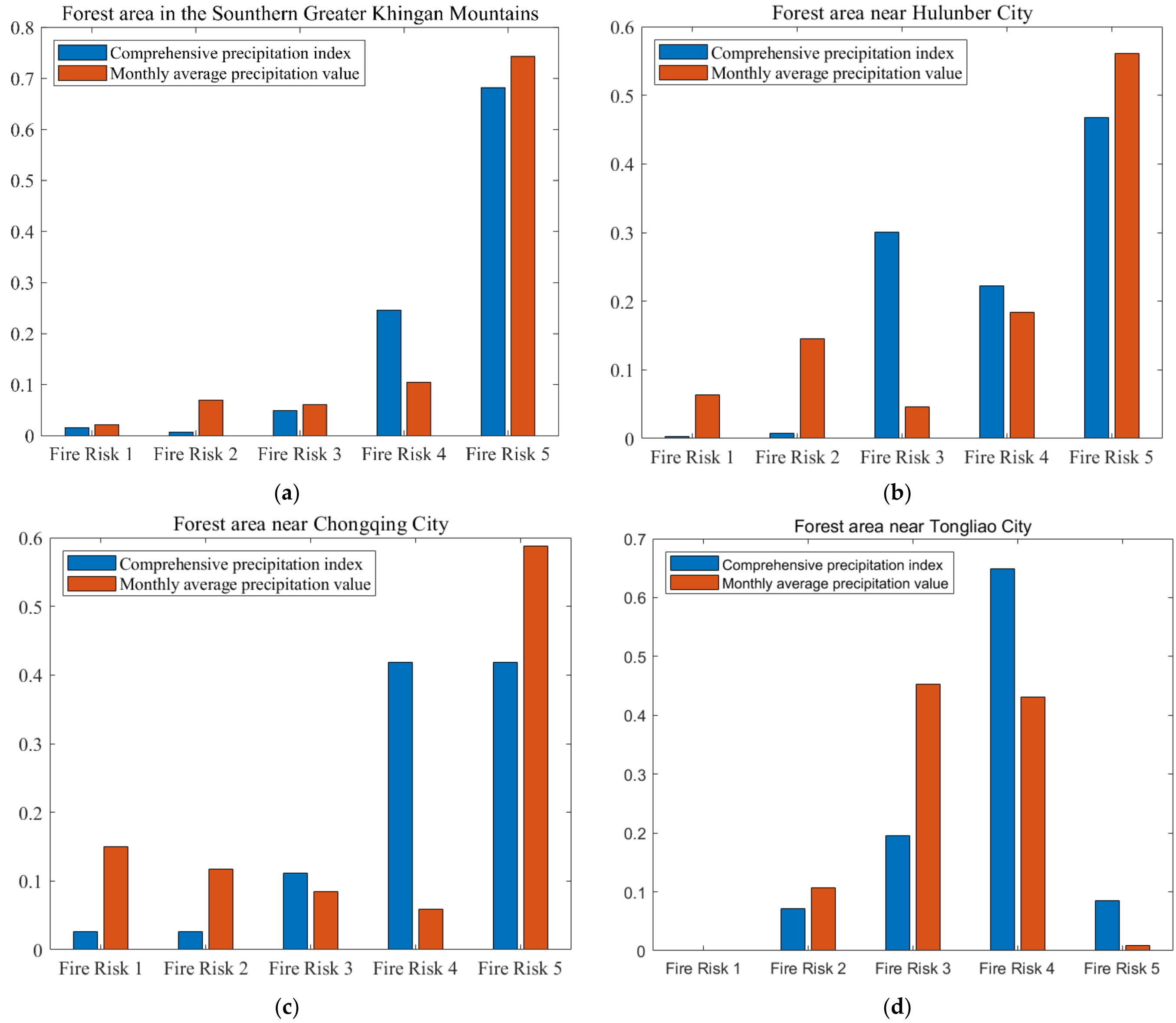

Figure 6. Proportion of fire points that fall within the forest fire danger rating map in four different forest areas in the test set trained by the two different methods: (**a**) forest area in the southern part of Greater Khingan Mountains; (**b**) forest area near Hulunber city; (**c**) forest area near Chongqing city; (**d**) forest area near Tongliao city.

The forest fire danger rating level map defined by the probability predicted by the ANN model is shown in Figure 8a–d, where the red points indicate the fire spots.

The proportion of fire spots in the test set falling on each fire danger rating map established by the three different methods is shown in Figure 9a–d.

Figure 9a–d show that compared to the logistic regression and the ANN neural network models, the accuracy of the SVM regression model is 5% higher than that of the other two machine learning models. Through comparison, it can be concluded that a regression model based on the comprehensive precipitation index calculated by a time-decaying model established in this study can predict forest fire danger rating levels with higher accuracy and better results.

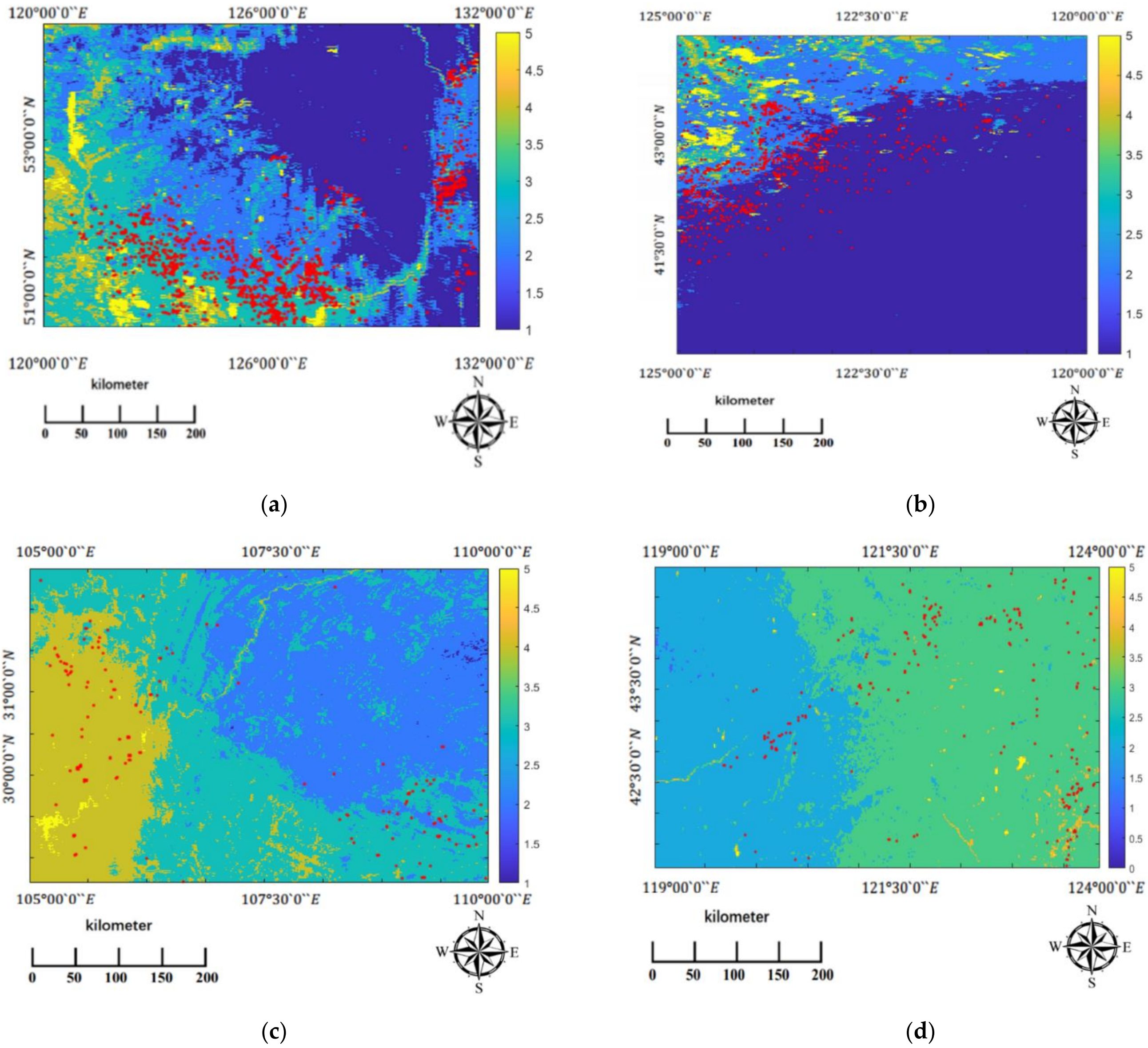

Figure 7. Forest fire danger rating map constructed by the logistic regression model: (**a**) forest area in the southern Greater Khingan Mountains; (**b**) forest area near Hulunber city; (**c**) forest area near Chongqing city; (**d**) forest area near Tongliao city.

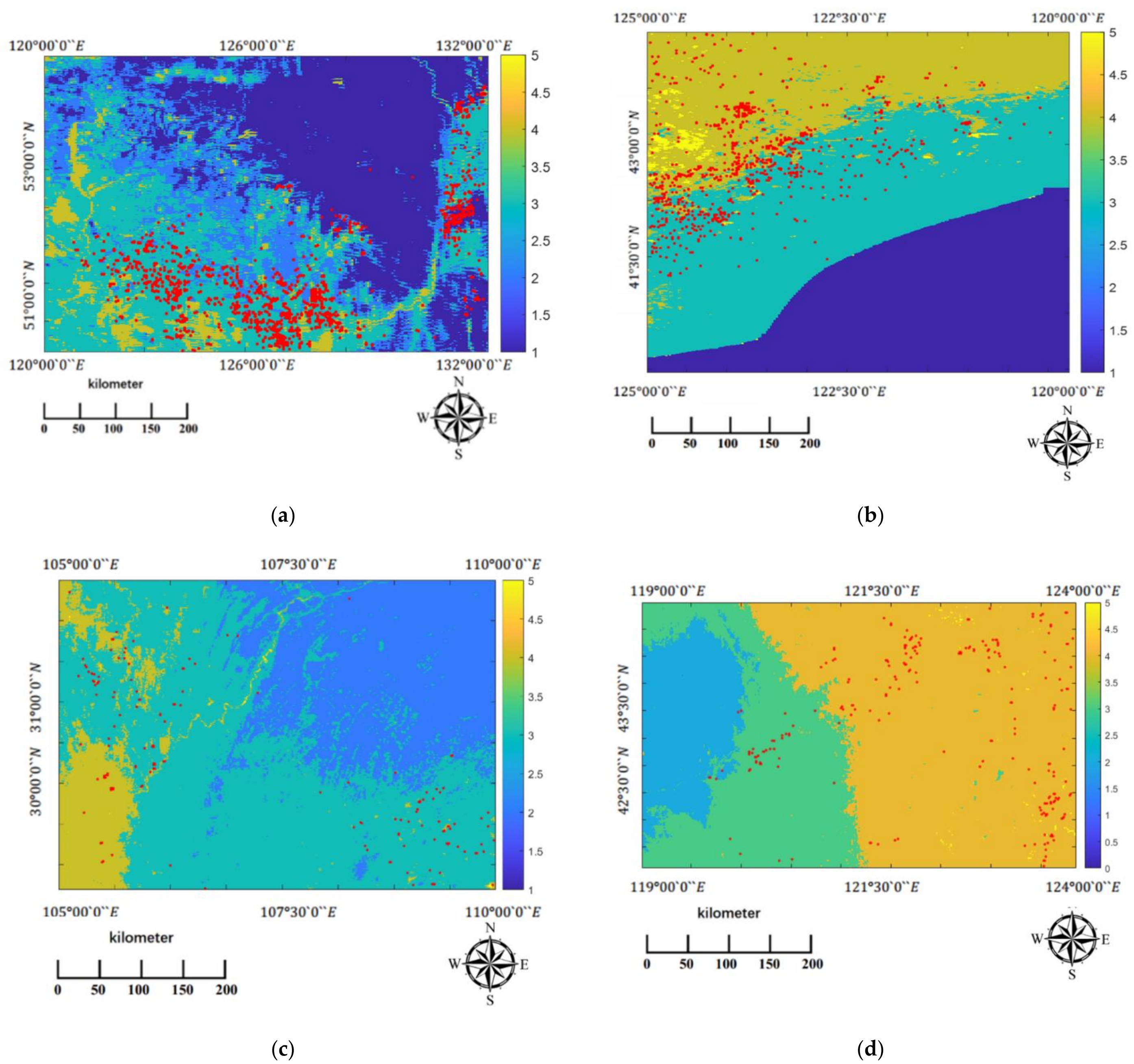

Figure 8. Forest fire danger rating map constructed by Artificial Neural Network (ANN) model: (**a**) forest area in the southern Greater Khingan Mountains; (**b**) forest area near Hulunbercity; (**c**) forest area near Chongqing city; (**d**) forest area near Tongliao city.

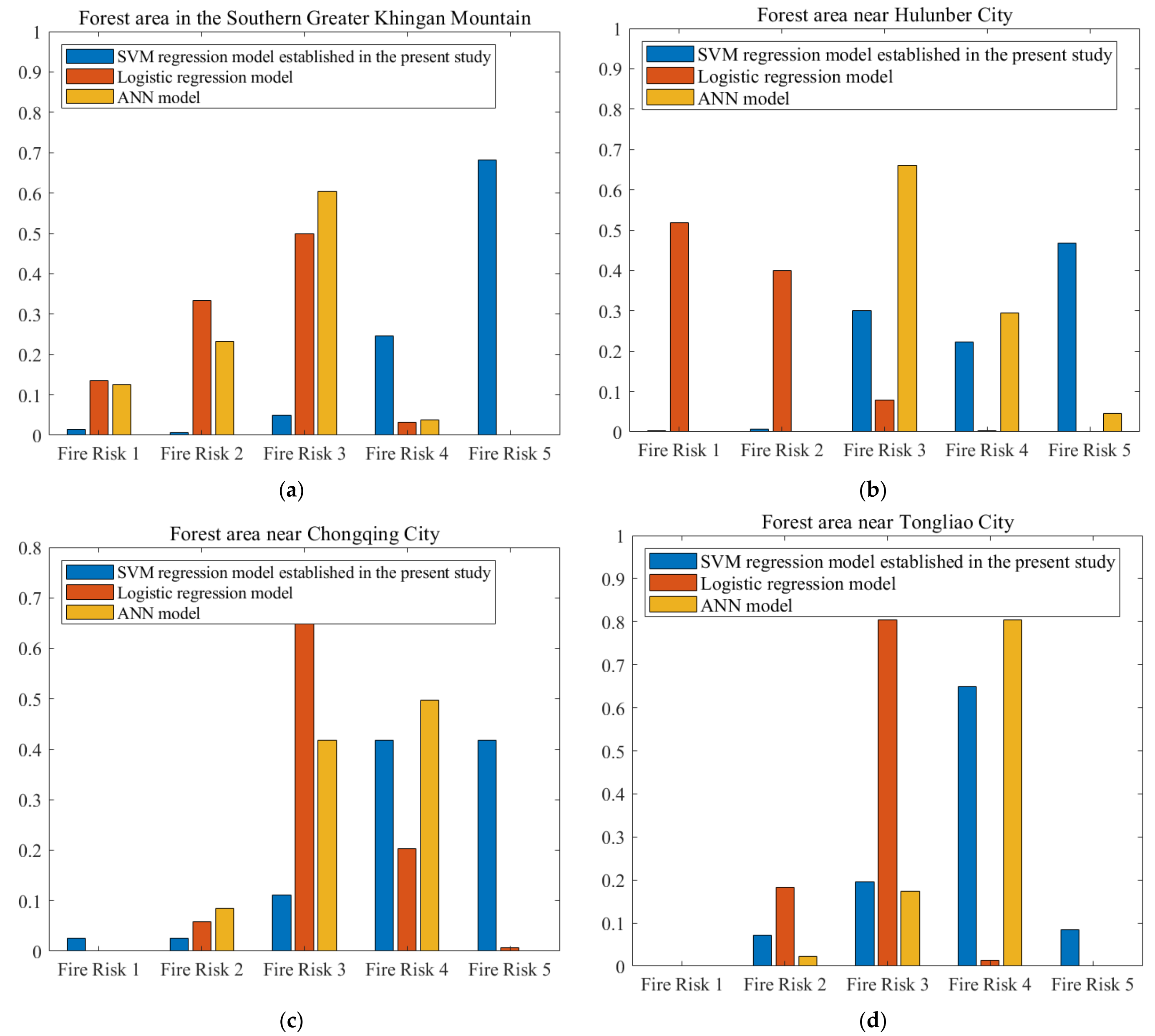

Figure 9. Proportion of forest fire points in the test set falling on each fire danger rating map established by three different methods: (**a**) forest area in the southern part of Greater Khingan Mountains; (**b**) forest area near Hulunber city; (**c**) forest area near Chongqing city; (**d**) forest area near Tongliao city.

Table 3 shows the mean squared error (MSE) value of using the four methods to build a forest fire warning model. The MSE value of the proposed method is the smallest, indicating that the model constructed by this method has a significant effect on predicting the risk of forest fire.

Table 3. Mean Squared Error (MSE) values of four methods used to build a forest fire warning model.

	SVM Regression Model from This Study	SVM Regression Model Using Monthly Precipitation	Logistic Regression Model	ANN Model
MSE	0.689	0.717	1.412	0.690

4. Conclusions

In this study, a new forest fire warning model was proposed. On the one hand, a time-decaying precipitation algorithm was used to calculate the comprehensive precipitation index instead of the traditional equal-weighting method, which is critical for fire prediction. The precipitation data used in this study was the "final-run" product of GPM_3IMERGDF, which is a type of precipitation data with high accuracy. In addition, the mutual information criterion was used to optimise the attenuation factor and the number of retrospective days in the modified model. As a result, the accuracy of fire risk prediction for the analyzed areas in central and northern China in the test set was improved by approximately 10%. The comprehensive precipitation index is calculated from the parameter, A, and the number of precipitation days, n, based on the forest dataset in central and northern China and the time-decaying precipitation model in this study. From Figure 1, we can see that the prediction is relatively more sensitive with respect to n than to A. On the other hand, the traditional fire point classification problem was converted into a fire point density regression problem through Gaussian convolution, which improved the rationality of the prediction method and the accuracy of the prediction result. In addition, the OOB principle of a random forest was adopted to select the independent variables of this model. The highest temperature, relative humidity, comprehensive precipitation index, and other factors of the day were selected as the independent variables of the SVM regression model. The method in this study was applied to four forest areas in central and northern China, with accuracies of 0.98, 0.99, 0.95, and 0.93, respectively. For comparison, this study applied the logistic regression and ANN models to the test dataset. The results showed that the SVM regression model based on the comprehensive precipitation index calculated by a time-decaying precipitation algorithm has a high accuracy. To demonstrate the applicability of our model for various areas, we select some areas with quite different climatic and geographical conditions in this study. For example, the forest area near Chongqing has a humid subtropical monsoon climate and belongs to the basin terrain, while the Greater Khingan Mountains belong to a continental monsoon climate in a cold temperate zone and belong to the plains and plateaus. The model in our study is suitable for predicting the fire risk in these forest areas with quite different climates and geographical conditions, which shows that the model has certain universality. If the model is used to predict forest fires risk in other forest areas, it may be necessary to select re-optimized parameters based on local actual data according to the method described in chapter 2.1–2.3 in this article. In this study, we used the SVM regression model to construct a forest fire prediction model. Deep learning is a machine learning method that has developed rapidly in recent years. In the case of sufficient samples, deep learning has better fitting and learning capabilities than SVM. How to combine the comprehensive precipitation index model in this paper based on the deep learning framework to achieve higher accuracy of predicting forest fire risk requires further investigation to be carried out in the future.

Supplementary Materials: The following supporting information can be downloaded at: https://www.mdpi.com/article/10.3390/f13030480/s1, Figure S1: Flowchart; Figure S2a: Forest fire spots in forest area in the southern part of Greater Khingan Mountains from 29 March to 13 April 2018; Figure S2b: Fire density of forest spots in forest area in the southern part of Greater Khingan Mountains from 29 March to 13 April 2018; Figure S3a: Daily maximum wind speed of forest area near the Oroqen Autonomous Banner from 4 April 2016; Figure S3b: Daily maximum temperature of forest area near the Oroqen Autonomous Banner from 4 April 2016; Figure S3c: NDVI of forest area near the Oroqen Autonomous Banner from 4 April 2016; Figure S3d: Relative Humidity of forest area near the Oroqen Autonomous Banner from 4 April 2016; Figure S3e: Altitude of forest area near the Oroqen Autonomous Banner from 4 April 2016; Figure S3f: VSWI of forest area near the Oroqen Autonomous Banner from 4 April 2016; Figure S4a: Predicted fire spots density map in forest area in the southern part of Greater Khingan Mountains on 29 March 2018; Figure S4b: Actual fire spots density map in forest area in the southern part of Greater Khingan Mountains on 29 March 2018; Figure S5a: Predicted fire spots density map in forest area near Hulunber City on 21 March 2015; Figure S5b: Actual fire spots density map in forest area near Hulunber City on 21 March 2015; Figure S6a: Predicted fire spots density map in forest area near ChongQing City on 8 March 2013; Figure S6b: Actual fire spots density map in forest area near ChongQing City on 8 March 2013; Figure S7a: Predicted fire spots density map in forest area near TongLiao City on 25 February 2019; Figure S7b: Actual fire spots density map in forest area near TongLiao City on 25 February 2019; Figure S8a: Daily maximum temperature of forest area near Hulunber city on 21 March 2015; Figure S8b: Daily maximum wind speed of forest area near Hulunber City on 21 March 2015; Figure S8c: Relative humidity of forest area near Hulunber City on 21 March 2015; Figure S8d: Comprehensive precipitation index of forest area near Hulunber City on 21 March 2015; Figure S8e: NDVI of forest area near Hulunber City on 21 March 2015; Figure S8f: VSWI of forest area near Hulunber City on 21 March 2015; Figure S8g: Altitude of forest area near Hulunber City on 21 March 2015; Figure S8h: Predicted fire spots density in the next fifteen days of forest area near Hulunber City on 21 March 2015.

Author Contributions: Formal analysis, J.C.; Methodology, J.C.; Resources, J.C.; Writing—original draft, J.C.; Writing—review and editing, X.W., Y.Y., X.Y., X.Q. and H.H. All authors have read and agreed to the published version of the manuscript.

Funding: This work was supported by the National Natural Science Foundation of China [No. 41976174], [No. 62071499], the Natural Science Foundation of Guangdong Province, China [No. 2020A1515010869], and the Natural Science Foundation of Guangdong Province, China [No. 2020A1515010869].

Data Availability Statement: Data are available on request from the corresponding author.

Conflicts of Interest: The authors declare no conflict of interest.

References

1. Chuvieco, E.; Aguado, I.; Yebra, M.; Nieto, H.; Salas, J.; Martín, M.P.; Vilar, L.; Martínez, J.; Martín, S.; Ibarra, P.; et al. Development of a framework for fire risk assessment using remote sensing and geographic information system technologies. *Ecol. Model.* **2010**, *221*, 46–58. [CrossRef]
2. Wang, X.; Deng, D.; Yi, H.; Xu, H.; Yang, S.; Zhang, H. Influences of pulse laser parameters on properties of AISI316L stainless steel thin-walled part by laser material deposition. *Opt. Laser Technol.* **2017**, *92*, 5–14. [CrossRef]
3. Hong, H.; Naghibi, S.A.; Dashtpagerdi, M.M.; Pourghasemi, H.R.; Chen, W. A comparative assessment between linear and quadratic discriminant analyses (LDA-QDA) with frequency ratio and weights-of-evidence models for forest fire susceptibility mapping in China. *Arab. J. Geosci.* **2017**, *10*, 167. [CrossRef]
4. Weike, L.; Jiyan, Y.; Zanquan, G.; Yajiao, G.; Tongxin, H. Analysis of forest fires in representative countries and regions in the world in 2019. *Fire Sci. Technol.* **2020**, *39*, 1280.
5. Binying, J. Temporal and Spatial Characteristics of Forest Fires in Northeast China from 2010 to 2019. *Shelter. For. Sci. Technol.* **2021**, *4*, 18–21. (In Chinese)
6. Turner, J.A.; Lawson, B.D. *Weather in the Canadian Forest Fire Danger Rating System. A User Guide to National Standards and Practices*; Pacific Forest Research Centre: Victoria, BC, Canada, 1984.
7. Bradshaw, L.S. *The 1978 National Fire-Danger Rating System: Technical Documentation*; US Department of Agriculture, Forest Service, Intermountain Forest and Range Experiment Station: Washington, DC, USA, 1984.
8. Bui, D.T.; Hoang, N.D.; Samui, P. Spatial pattern analysis and prediction of forest fire using new machine learning approach of Multivariate Adaptive Regression Splines and Differential Flower Pollination optimization: A case study at Lao Cai province (Viet Nam). *J. Environ. Manag.* **2019**, *237*, 476–487. [CrossRef]
9. Müller, M.M.; Vilà-Vilardell, L.; Vacik, H. Towards an integrated forest fire danger assessment system for the European Alps. *Ecol. Inform.* **2020**, *60*, 101151. [CrossRef]
10. Zheng, Z.; Gao, Y.; Yang, Q.; Zou, B.; Xu, Y.; Chen, Y.; Yang, S.; Wang, Y.; Wang, Z. Predictingforest fire risk based on mining rules with ant-miner algorithm in cloud-rich areas. *Ecol. Indic.* **2020**, *118*, 106772. [CrossRef]
11. Zhiwei, X. Assessing the Impact of Climate Change on Forest Fire in Nepal Based on Time Series Remote Sensing Data. Master's Thesis, Jiangxi University of Science and Technology, Ganzhou, China, 2019. (In Chinese).
12. Maki, M.; Ishiahra, M.; Tamura, M. Estimation of leaf water status to monitor the risk of forest fires by using remotely sensed data. *Remote Sens. Environ.* **2004**, *90*, 441–450. [CrossRef]
13. Zhang, G.; Wang, M.; Liu, K. Forest fire susceptibility modeling using a convolutional neural network for Yunnan province of China. *Int. J. Disaster Risk Sci.* **2019**, *10*, 386–403. [CrossRef]
14. Mohajane, M.; Costache, R.; Karimi, F.; Pham, Q.B.; Essahlaoui, A.; Nguyen, H.; Laneve, G.; Oudija, F. Application of remote sensing and machine learning algorithms for forest fire mapping in a Mediterranean area. *Ecol. Indic.* **2021**, *129*, 107869. [CrossRef]
15. Wu, Y. Accuracy Evaluation and Comparison of GPM IMERG v5 and TRMM 3B42v7 Precipitation Product in the Yangtze River Basin. Master's Thesis, Nanjing Forestry University, Nanjing, China, 2019. [CrossRef]

16. Arshad, M.; Ma, X.; Yin, J.; Ullah, W.; Ali, G.; Ullah, S.; Liu, M.; Shahzaman, M.; Ullah, I. Evaluation of GPM-IMERG and TRMM-3B42 precipitation products over Pakistan. *Atmos. Res.* **2021**, *249*, 105341. [CrossRef]
17. Thach, N.N.; Ngo, D.B.; Xuan-Canh, P.; HongThi, N.; Thi, B.H.; NhatDuc, H.; Dieu, T.B. Spatial pattern assessment of tropical forest fire danger at Thuan Chau area (Vietnam) using GIS-based advanced machine learning algorithms: A comparative study. *Ecol. Inform.* **2018**, *46*, 74–85. [CrossRef]
18. Wang, J.; Ye, G.; Li, L.; Xu, Z.; Yue, Y. Fine Meteorological Grade Forecast for Forest Fire Risk in Fujian. *Chin. J. Agrometeorol.* **2010**, *31*, 129.
19. Çolak, E.; Sunar, F. Evaluation of forest fire risk in the Mediterranean Turkish forests: A case study of Menderes region, Izmir. *Int. J. Disaster Risk Reduct.* **2020**, *45*, 101479. [CrossRef]
20. Eugenio, F.; dos Santos, A.; Fiedler, N.; Ribeiro, G.; da Silva, A.; dos Santos, Á.; Paneto, G.; Schettino, V. Applying GIS to develop a model for forest fire risk: A case study in Espírito Santo, Brazil. *J. Environ. Manag.* **2016**, *173*, 65–71. [CrossRef]
21. Bui, D.T.; Bui, Q.T.; Nguyen, Q.P.; Pradhan, B.; Nampak, H.; Trinh, P.T. A hybrid artificial intelligence approach using GIS-based neural-fuzzy inference system and particle swarm optimization for forest fire susceptibility modeling at a tropical area. *Agric. For. Meteorol.* **2017**, *233*, 32–44. [CrossRef]
22. Arpaci, A.; Malowerschnig, B.; Sass, O.; Vacik, H. Using multi variate data mining techniques for estimating fire susceptibility of Tyrolean forests. *Appl. Geogr.* **2014**, *53*, 258–270. [CrossRef]
23. Oliveira, S.; Oehler, F.; San-Miguel-Ayanz, J.; Camia, A.; Pereira, J.M. Modeling spatial patterns of fire occurrence in Mediterranean Europe using Multiple Regression and Random Forest. *For. Ecol. Manag.* **2012**, *275*, 117–129. [CrossRef]
24. Guo, F.; Zhang, L.; Jin, S.; Tigabu, M.; Su, Z.; Wang, W. Modeling anthropogenic fire occurrence in the boreal forest of China using logistic regression and random forests. *Forests* **2016**, *7*, 250. [CrossRef]
25. Koutsias, N.; Kalabokidis, K.D.; Allgöwer, B. Fire occurrence patterns at landscape level: Beyond positional accuracy of ignition points with kernel density estimation methods. *Nat. Resour. Model.* **2004**, *17*, 359–375. [CrossRef]
26. Monjarás-Vega, N.A.; Briones-Herrera, C.I.; Vega-Nieva, D.J.; Calleros-Flores, E.; Corral-Rivas, J.J.; López-Serrano, P.M.; Pompa-García, M.; Rodríguez-Trejo, D.A.; Carrillo-Parra, A.; González-Cabán, A.; et al. Predicting forest fire kernel density at multiple scales with geographically weighted regression in Mexico. *Sci. Total Environ.* **2020**, *718*, 137313. [CrossRef]
27. Hurley, J.F. An application of Newton's law of cooling. *Math. Teach.* **1974**, *67*, 141–142. [CrossRef]
28. Zaitchik, B.F.; Santanello, J.A.; Kumar, S.V.; Peters-Lidard, C.D. Representation of soil moisture feedbacks during drought in NASA Unified WRF (NU-WRF). *J. Hydrometeorol.* **2013**, *14*, 360–367. [CrossRef]
29. Gillett, N.; Weaver, A.; Zwiers, F.; Flannigan, M. Detecting the effect of climate change on Canadian forest fires. *Geophys. Res. Lett.* **2004**, *31*, L18211. [CrossRef]
30. Heimann, M.; Reichstein, M. Terrestrial ecosystem carbon dynamics and climate feedbacks. *Nature* **2008**, *451*, 289–292. [CrossRef]
31. Guttman, N.B. *Comparing the Palmer Drought Index and the Standardized Precipitation Index1*; Wiley Online Library: Hoboken, NJ, USA, 1998.
32. Camp, A.; Oliver, C.; Hessburg, P.; Everett, R. Predicting late-successional fire refugia pre-dating European settlement in the Wenatchee Mountains. *For. Ecol. Manag.* **1997**, *95*, 63–77. [CrossRef]
33. Nami, M.H.; Jaafari, A.; Fallah, M.; Nabiuni, S. Spatial prediction of wildfire probability in the Hyrcanian ecoregion using evidential belief function model and GIS. *Int. J. Environ. Sci. Technol.* **2018**, *15*, 373–384. [CrossRef]
34. Tehrany, M.S.; Jones, S.; Shabani, F.; Martínez-Álvarez, F.; Bui, D.T. A novel ensemble modeling approach for the spatial prediction of tropical forest fire susceptibility using LogitBoost machine learning classifier and multi-source geospatial data. *Theor. Appl. Climatol.* **2019**, *137*, 637–653. [CrossRef]
35. Bajocco, S.; Dragoz, E.; Gitas, I.; Smiraglia, D.; Salvati, L.; Ricotta, C. Mapping forest fuels through vegetation phenology: The role of coarse-resolution satellite time-series. *PLoS ONE* **2015**, *10*, e0119811. [CrossRef]
36. Liu, X.L.; Zhou, T.G.; Wen, L.; Lang, W.U.; Zhang, L. Research on drought characteristics of Henan Province from 2000 to 2016 based on VSWI and SPI. *Arid. Land Geogr.* **2018**, *41*, 8. (In Chinese) [CrossRef]
37. Criminisi, A.; Shotton, J.; Konukoglu, E. Decision forests: A unified framework for classification, regression, density estimation, manifold learning and semi-supervised learning. *Found. Trends® Comput. Graph. Vis.* **2012**, *7*, 81–227. [CrossRef]
38. Smola, A.J.; Schölkopf, B. A tutorial on support vector regression. *Stat. Comput.* **2004**, *14*, 199–222. [CrossRef]
39. Ruoyun, N.; Panmao, Z.; Minghua, S. A review of forest fire danger meteorological index and its construction methods. *Meteorology* **2006**, *12*, 3–9. (In Chinese)
40. Baral, P.; Haq, M.A. Spatial prediction of permafrost occurrence in Sikkim Himalayas using logistic regression, random forests, support vector machines and neural networks. *Geomorphology* **2020**, *371*, 107331. [CrossRef]
41. Achu, A.L.; Thomas, J.; Aju, C.D.; Gopinath, G.; Kumar, S.; Reghunath, R. Machine-learning modelling of fire susceptibility in a forest-agriculture mosaic landscape of southern India. *Ecol. Inform.* **2021**, *64*, 101348. [CrossRef]
42. Maeda, E.E.; Formaggio, A.R.; Shimabukuro, Y.E.; Arcoverde, G.F.; Hansen, M.C. Predicting forest fire in the Brazilian Amazon using MODIS imagery and artificial neural networks. *Int. J. Appl. Earth Obs. Geoinf.* **2009**, *11*, 265–272. [CrossRef]

43. Ouache, R.; Nahiduzzaman, K.M.; Hewage, K.; Sadiq, R. Performance investigation of fire protection and intervention strategies: Artificial neural network-based assessment framework. *J. Build. Eng.* **2021**, *42*, 102439. [CrossRef]
44. de Bem, P.P.; de Carvalho Júnior, O.A.; Matricardi, E.A.; Guimarães, R.F.; Gomes, R.A. Predicting wildfire vulnerability using logistic regression and artificial neural networks: A case study in Brazil's Federal District. *Int. J. Wildland Fire* **2018**, *28*, 35–45. [CrossRef]
45. Satir, O.; Berberoglu, S.; Donmez, C. Mapping regional forest fire probability using artificial neural network model in a Mediterranean forest ecosystem. *Geomat. Nat. Hazards Risk* **2016**, *7*, 1645–1658. [CrossRef]